Geophysical Research Letters

RESEARCH LETTER
10.1029/2023GL104822

Ocean Carbon Dioxide Uptake in the Tailpipe of Industrialized Continents

J. B. Palter[1], S. Nickford[1], and L. Mu[1,2]

[1]Graduate School of Oceanography, University of Rhode Island, Narragansett, RI, USA, [2]Cooperative Institute for Climate, Ocean, and Ecosystem Studies, University of Washington, Seattle, WA, USA

Key Points:

- Atmospheric CO_2 is elevated downwind of highly industrialized continents, the "tailpipe regions," east of Asia and North America
- Atmospheric CO_2 anomalies swept over the neighboring ocean enhance ocean uptake above estimates using zonal mean atmospheric CO_2
- Errors average out over hemispheric-scales, but introduce important biases on local scales

Correspondence to:

J. B. Palter,
jpalter@uri.edu

Citation:

Palter, J. B., Nickford, S., & Mu, L. (2023). Ocean carbon dioxide uptake in the tailpipe of industrialized continents. *Geophysical Research Letters*, *50*, e2023GL104822. https://doi.org/10.1029/2023GL104822

Received 3 JUN 2023
Accepted 6 SEP 2023

Author Contributions:

Conceptualization: J. B. Palter, S. Nickford
Data curation: S. Nickford, L. Mu
Formal analysis: J. B. Palter
Funding acquisition: J. B. Palter
Investigation: L. Mu
Methodology: J. B. Palter, S. Nickford
Project Administration: J. B. Palter
Supervision: J. B. Palter
Validation: L. Mu
Visualization: J. B. Palter, S. Nickford
Writing – original draft: J. B. Palter
Writing – review & editing: J. B. Palter, S. Nickford, L. Mu

Abstract A simplifying assumption in many studies of ocean carbon uptake is that the atmosphere is well-mixed, such that zonal variations in its carbon dioxide (CO_2) content can be neglected in the calculation of air-sea fluxes. Here, we examine this assumption at various scales to quantify the errors it introduces. For global annual averages, we find that positive and negative errors effectively cancel, so the use of atmospheric zonal-average CO_2 introduces reassuringly small errors in fluxes. However, for millions of square kilometers of the North Pacific and Atlantic that are downwind of the highly industrialized northern hemisphere continents, these biases average to over 6% of the annual ocean uptake and can cause errors of up to 30% on a given day. This work highlights the need to use a high quality, spatially-resolved atmospheric CO_2 product for process studies and for accurate long-term average maps of ocean carbon uptake.

Plain Language Summary Closing the global carbon budget is key to keeping tabs on society's progress toward a stabilized climate. Therefore, oceanographers go to great lengths to reduce uncertainty in the quantification of ocean carbon uptake. While there has been much attention on improving almost every aspect of the calculation of air-sea exchange of carbon dioxide, one aspect has been seldom examined: How atmospheric carbon dioxide (CO_2) concentrations vary across the globe. For instance, westerly winds draw elevated CO_2 from Asia and North America over the neighboring oceans. This promotes higher ocean CO_2 uptake than would be estimated if we neglect that spatial variation. Luckily, the errors introduced by ignoring spatial variability average to a very small number over large enough scales (though this was not a foregone conclusion, given that the elevated atmospheric concentrations are found over very windy, high ocean uptake regions). However, in the "tailpipe" of the industrialized continents (i.e., the western North Pacific and North Atlantic), neglecting the elevated atmospheric CO_2 concentrations would lead to a low bias in ocean carbon uptake estimates. Overall, the work suggests that local ocean carbon uptake studies should measure atmospheric CO_2 locally or make use of atmospheric CO_2 estimates that resolve spatial variability.

1. Introduction

The contemporary ocean absorbs about 25% of anthropogenic CO_2 emissions each year (Friedlingstein et al., 2022), which helps determine the pace of climate change. This ocean sink represents the integrated air-sea flux across the entire global ocean. However, at any time or place, the ocean can absorb or release CO_2 (Figure 1a). For given wind and sea state conditions, the flux of CO_2 into or out of the ocean is determined by the difference in the partial pressure of CO_2 between the ocean surface and the lower atmosphere (e.g., Wanninkhof, 2014). Because the surface ocean partial pressure of CO_2 (pCO_2^{sw}) varies by a much larger amount than the atmospheric partial pressure (pCO_2^{atm}) (Figure 1), the influence of atmospheric pCO_2 variability on ocean carbon uptake has only rarely been explored (Northcott et al., 2019; Wanninkhof et al., 2019).

Nevertheless, sources and sinks of CO_2 to the atmosphere cause persistent spatial gradients of the gas, most evident when viewing the mixing ratio of CO_2 in the dry atmosphere (χCO_2^{atm} anomaly, Figure 1d). The mixing ratio and partial pressure of CO_2 can be related via the following equation:

$$pCO_2^{atm} = \chi CO_2^{atm} * (P_{atm} - pH_2O) \quad (1)$$

where P_{atm} is the barometric pressure at sea level, and pH_2O is the partial pressure of water vapor in the atmosphere. Mapping χCO_2^{atm} provides a picture of the role of spatially-varying sources and sinks of CO_2.

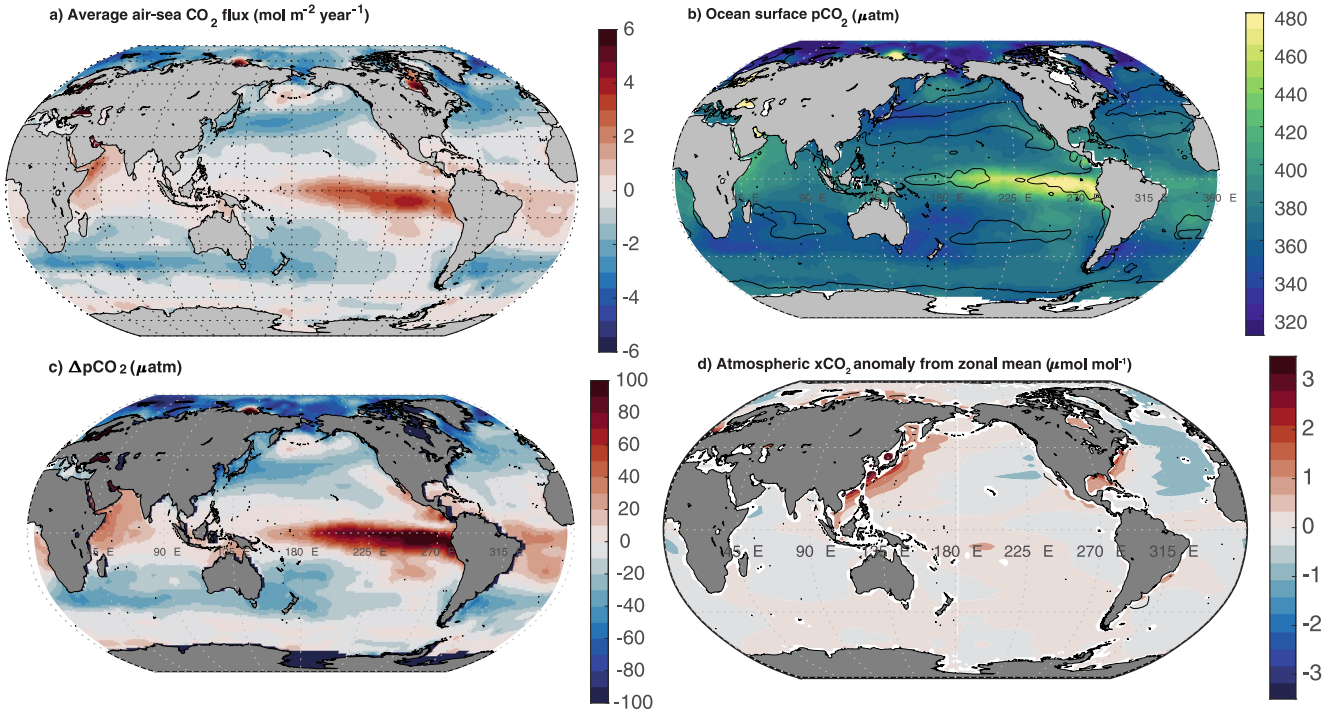

Figure 1. Air-sea flux of CO_2 (negative indicates ocean uptake) and the surface ocean and lower atmosphere CO_2 averaged over the years 2000–2018. (a) Air-sea CO_2 flux in mol m^{-2} $year^{-1}$ calculated with ocean properties from Jersild et al. (2023) based on the methods of Landschützer et al. (2013, 2016, 2020) and atmospheric properties from CT2022, as described in the text and Table 1. (b) Surface ocean pCO_2 from Jersild et al. (2023) (μatm). (c) $(\Delta pCO_2) = pCO_2^{sw} - pCO_2^{atm}$ (μatm) with pCO_2^{sw} from Jersild et al. (2023) and pCO_2^{atm} from CT2022. (d) Surface CO_2 mixing ratio in dry air (χCO_2) anomaly relative to a zonal mean at each latitude, calculated from CT2022.

When calculating air-sea carbon exchange, it is commonly assumed that χCO_2^{atm} is constant over large spatial scales. Many of the air-sea flux reconstructions that inform the Global Carbon Project's annual budget exercise (Friedlingstein et al., 2022), as well as recent work to facilitate the intercomparison among these reconstructions (Fay et al., 2021), use a monthly, zonal average atmospheric χCO_2^{atm} in 3° latitude bins (NOAA's surface marine boundary layer CO_2 product, https://gml.noaa.gov/ccgg/mbl/mbl.html). Using a zonal, monthly mean product neglects the spatial structure and submonthly variability in atmospheric χCO_2^{atm}.

A map of time-mean anomalies in χCO_2^{atm} from the zonal mean (Figure 1d) highlights that the predominantly westerly winds draw elevated χCO_2^{atm} over the ocean near the east coasts of North America and Asia, but not along the western margins of the continents (e.g., Western Europe). Here, we call this downwind region, the *tailpipe* of the industrialized continents. Although time-mean χCO_2^{atm} anomalies from the zonal mean are less than +5 μatm, the strong ocean uptake in these regions is driven by atmosphere-ocean pCO_2 differences (ΔpCO_2) with an average magnitude of less than 40 μatm (Figure 1). Neglecting this spatial structure systematically underestimates ΔpCO_2 in the *tailpipe regions* to cause a local underestimate of ocean carbon uptake. Our goal is to quantify the role of these local, persistent, positive atmospheric χCO_2^{atm} anomalies on air-sea CO_2 exchange.

We first hypothesized that atmospheric χCO_2 anomalies create an unrecognized bias in flux estimates during a deployment of three Saildrone uncrewed surface vehicles from Newport, Rhode Island in December 2021. These vehicles were equipped with an ASVCO2 system, capable of measuring atmosphere and surface ocean χCO_2 with an accuracy of 2 μmol mol^{-1} (Nickford et al., 2022; Sabine et al., 2020; Sutton et al., 2021). While the three vehicles were still within 30 km of land and sailing in a tight formation to provide inter-vehicle comparison data, they sampled an atmospheric χCO_2 anomaly >50 μmol mol^{-1} above background values (Figure 2). The spike was so unusual among the hundreds of drone-days of data collected that we might have wrongly assumed it was due to a sensor error if only one vehicle had observed it. Yet, the larger spatial context provided by NOAA's CarbonTracker, version CT2022 (Jacobson et al., 2023; Peters et al., 2007), shows that the terrestrial northeastern US saw daily atmospheric χCO_2 values elevated approximately to level of the spike (Figure 2a). These anomalies can be advected over the ocean before they are mixed with cleaner air further from land-based CO_2 sources. The CT2022 Near-Real

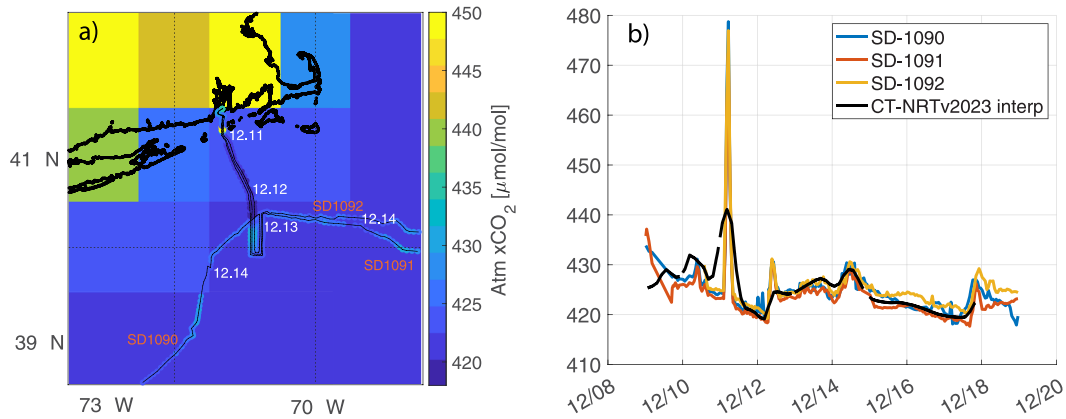

Figure 2. Comparison of surface χCO_2 from CT2022 and that measured aboard three Saildrone vehicles in December 2021. (a) Map of CT2022 NearRealTime North America 1° × 1° latitude × longitude product χCO_2 (μmol mol^{-1}) at 0430 UTC 11 December 2021, approximately the time that the Saildrone vehicles encountered the largest atmospheric anomaly (>475 μmol mol^{-1}) of the multi-month mission. The first 5 days of the Saildrone χCO_2 observations are plotted on top of the map using the same color scale, so they are most visible when they differ from the CT2022 product. Saildrone vehicle numbers (SD1090, 1091, and 1092) are written in orange and the location where each vehicle was at midnight of a given day is denoted in white text. (b) A time series view of the first 9 days of each Saildrone χCO_2 data (colored lines) and CT2022 interpolated to the time and location of vehicle 1091 (black line).

Time North America product (Jacobson et al., 2023; Peters et al., 2007), interpolated to the time and location of one of the Saildrone vehicles is generally within 5 μmol mol^{-1} of the direct measurements (Figure 2b). The product reproduces an elevated χCO_2 level at the time and location of the large spike, although at a lower level, as might be expected given that the anomaly was observed in a fraction of the product's 1° grid (Figure 2a).

Here, we use the CT2022 global atmospheric inversion to explore the influence of spatial variability in atmospheric CO_2 on estimates of air-sea carbon fluxes. CT2022 resolves spatial and temporal variations in atmospheric χCO_2 that arise due to changes in CO_2 sources and sinks. Fluctuations due to industrial and transportation emissions, as well as CO_2 drawdown in spring by the terrestrial biosphere, lead to considerable variability in Northern Hemisphere atmospheric χCO_2 (Jacobson et al., 2023; Peters et al., 2007). In the next section, we briefly describe the data products and our analysis methods. Section 3.1 addresses the influence of χCO_2^{atm} spatial gradients on global and basin-scale estimates of ocean CO_2 uptake. In Section 3.2, we focus specifically on the *tailpipe regions* to highlight the important local errors caused by neglecting atmospheric χCO_2^{atm} variability. Finally, Section 4 offers a summary and recommendations for future work.

2. Data Sources and Methods

The CarbonTracker project (Jacobson et al., 2023; Peters et al., 2007) assimilates atmospheric χCO_2^{atm} observations made at 460 time series locations around the world to optimize the results from an atmospheric transport model. The Saildrone ASVCO2 data presented in Figure 2 were not part of the assimilated data. In the analysis that follows, we use the delayed time CarbonTracker, version CT2022, global product with a 3° × 2° latitude/longitude resolution and 8 time steps each day, averaged daily to reduce processing time. At the time of writing, there were 19 complete years from 2000 to 2018. CT2022 also provides the atmospheric pressure and humidity information necessary to calculate pCO_2^{atm} (Equation 1).

The exchange of CO_2 over the ice-free ocean can be estimated through the bulk formula (e.g., Ho et al., 2006, 2011; Wanninkhof, 2014):

$$F = 7.7 \times 10^{-4} \left\langle U^2 \right\rangle \left(pCO_2^{sw} - pCO_2^{atm} \right) \quad (2)$$

where $\langle U^2 \rangle$ is the average of the neutral stability winds at 10 m height here approximated as the lowest layer winds in CT2022, and pCO_2 is the partial pressure of CO_2 at the ocean's surface (pCO_2^{sw}) or in the marine boundary layer (pCO_2^{atm}), the latter assumed equal to the pCO_2 at the CT2022 level closest to the ocean's surface. Because neither CT2022 nor the Landschützer ocean pCO_2 product (made available by Jersild et al. (2023)) provide sea surface temper-

Table 1
Parameter Choices to Solve for Fluxes via Equations 1 and 2, for the Full Flux and Flux With $\chi CO_2^{\mathcal{M}\_atm}$

Parameter	Full flux	Flux with $\chi CO_2^{\mathcal{M}\_atm}$
χCO_2^{atm}, $\langle U^2 \rangle$	Lowest vertical level global CT2022 at 3° lat × 2° lon resolution, averaged daily	Zonal average of global CT2022 in 3° latitude bins, averaged daily
P_{atm}, pH_2O	CT2022 global, daily mean at 3° × 2° lat, lon resolution	Same as *full flux*
pCO_2^{sw}	Data provided by Jersild et al. (2023); methods from Landschützer et al. (2013, 2020)	Same as *full flux*

ature, we use the simplifying assumption that the product of the Schmidt number and solubility are roughly temperature invariant and can be approximated by the constant 7.7×10^{-4} when U is in m s^{-1} and pCO_2 in µatm (Wanninkhof, 2014).

To calculate fluxes in this work (Equation 2), pCO_2^{atm} is interpolated from the 3 × 2° resolution of CT2022 to the 1° × 1° resolution of Jersild et al. (2023).

For the *full flux* calculation, we use daily-mean CT2022 χCO_2^{atm} that varies with latitude and longitude. For the *flux with* $\chi CO_2^{\mathcal{M}\_atm}$, all parameters in Equations 1 and 2 are the same as for the *full flux,* except for χCO_2^{atm}, which is replaced by the zonal mean of the daily-mean CT2022 product in every 3° latitude band. All parameter choices are listed in Table 1. With these choices, the comparison of *full flux* versus the *flux with* $\chi CO_2^{\mathcal{M}\_atm}$ provides a quantification of the role of zonal variability in χCO_2^{atm} on the air-sea exchange of CO_2.

3. Results and Discussion

3.1. Low Bias at Global to Basin Scales

Part of our initial hypothesis was that neglecting zonal variability in χCO_2^{atm} could rectify into a possibly important bias in large-scale fluxes, since the neglected positive χCO_2^{atm} anomalies are found above windy, high ocean uptake regions (compare Figures 1a–1d). This hypothesis was not supported at the global scale: The fluxes integrated over these largest scales is almost identical whether using the full χCO_2^{atm} product or its zonal mean in the calculation (Table 2). Even narrowing over to just the northern hemisphere, where the zonal gradients in χCO_2^{atm} are largest, neglecting zonal variability in χCO_2^{atm} introduces extremely small differences in the ocean carbon uptake. In other words, over large enough scales, underestimated and overestimated flux average to a very small number. It is only when we zoom to the *tailpipe* regions that the biases start to be a more substantial fraction of the total flux (Figure 3). It should be noted that CT2022 has been shown to underestimate χCO_2^{atm} under poorly mixed atmospheric conditions, like those found within 100 km of the shore in Monterey Bay (Northcott et al., 2019), and this possible bias is outside our analysis.

3.2. Ocean CO_2 Uptake Underestimated in *Tailpipe* Regions

Figure 3 shows the time-mean *full flux* and the bias that results from using $\chi CO_2^{\mathcal{M}\_atm}$ in the flux calculation. These biases are greater than 0.05 mol m^{-2} $year^{-1}$ along the east coasts of both highly industrialized northern hemisphere continents (Figure 3b). Across these regions, the mean flux into the ocean is substantially underestimated (Figure 3b; Table 2). Moreover, the biases extend over large swaths of ocean, amounting to over 1 million km^2 of the North Atlantic and 8 million km^2 of the North Pacific (about half as large and 4 times larger than the area of Greenland, respectively).

Figure 3b also shows that the largest overestimate of ocean carbon uptake using a zonal mean atmospheric χCO_2 is in the eastern North Atlantic. The cause is apparent in Figure 1d, which shows that the lowest above-ocean surface χCO_2 anomalies relative to the zonal mean occur over the eastern North Atlantic from about 25° to 50°N. Why atmospheric χCO_2 is lowest at these longitudes relative to the zonal mean is an open question. Though a detailed investigation is beyond the scope of this work, we speculate that the proximity to the strong ocean sink region in the subpolar North Atlantic (e.g., Sabine et al., 2004) may be one cause. The Lagrangian back-trajectories of air parcels that arrive at the surface of the eastern North Atlantic have a strong component

Table 2
CO_2 Fluxes (GtC Year^{-1} ± the Standard Deviation of the Daily Values) for the 2000–2018 Time-Mean Full Flux and Flux With $\chi CO_2^{ZM\_atm}$ for Different Integration Regions

Areas	Full flux* (GtC year^{-1})	Flux with $\chi CO_2^{ZM_{atm}}$ (GtC year^{-1})	Percent difference
Global	−1.80 ± 0.81	−1.79 ± 0.80	0.24%
Northern Hemisphere	−0.95 ± 0.72	−0.94 ± 0.71	0.74%
NA Tailpipe (1.3e6 km^2)	−0.018 ± 0.03	−0.017 ± 0.03	6.13%
Asia Tailpipe (8.5e6 km^2)	−0.129 ± 0.09	−0.120 ± 0.08	7.52%
Case studies	**Full flux (mol m^{-2} yr^{-1})**	**Flux with $\chi CO_2^{ZM_{atm}}$ (mol m^{-2} yr^{-1})**	**Percent difference**
Scotian Shelf (2014) 43°N, 67.5°W	−1.70	−1.62	4.9%
East China Sea (2014) 43°N, 67.5°W	−1.28	−1.09	17.5%

Note. The North American and Asian *tailpipe* regions are integrated over the regions outlined in Figure 3b.

from the Labrador Sea, and this component has increased since 1996 when the Atlantic Multidecadal Oscillation switched to a predominantly positive phase (Yamamoto & Palter, 2016).

Using Figure 3, we define a *tailpipe* contour as the region where the time-mean *full flux* exceeds the *flux with* $\chi CO_2^{ZM\_atm}$ by at least 0.05 mol m^{-2} year^{-1}. The time-mean fluxes integrated over these *tailpipe regions* are given in Table 2. Calculating air-sea CO_2 exchange with the zonally-averaged χCO_2^{atm} results in >6% underestimate of the 2000–2018 mean ocean uptake averaged over these *tailpipe regions*. Because of the large size of the Asian *tailpipe region*, the area-integrated ocean CO_2 uptake bias is over 7 times larger than the North American *tailpipe region*. In addition to this time-mean bias, a large error would be introduced for calculations over short periods, analogous to studies calculating fluxes during field campaigns. The maximum daily ocean uptake underestimates

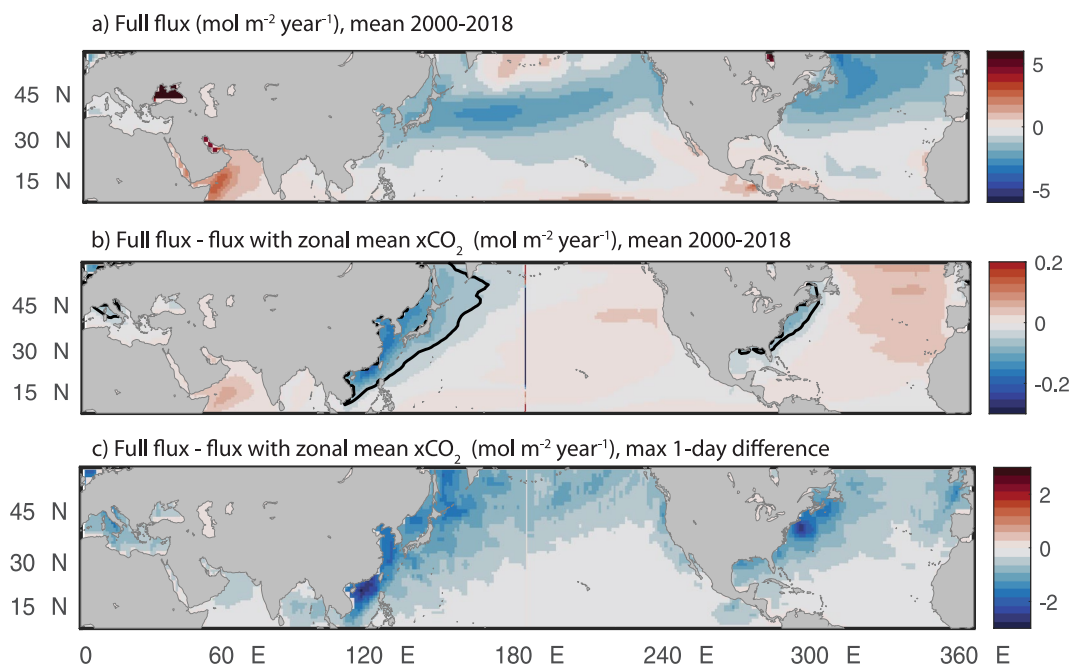

Figure 3. CO_2 flux and flux errors in the Northern Hemisphere and *tailpipe regions.* (a) Average *full flux* in mol m^{-2} year^{-1}. (b) *Full flux* minus *flux with* $\chi CO_2^{ZM\_atm}$ averaged over the years 2000–2018. Negative values are regions where *flux with* $\chi CO_2^{ZM\_atm}$ underestimates ocean uptake. Dark contour is where ocean uptake underestimate is ≥0.05 mol m^{-2} year, which defines the *tailpipe contour* used in Table 2. (c) Maximum one-day ocean uptake underestimate (i.e., the biggest negative daily difference of *flux with* $\chi CO_2^{ZM\_atm}$ minus *full flux*). Units are in mol m^{-2} year^{-1} for comparison to other panels, calculated by multiplying the daily underestimate by 365 days.

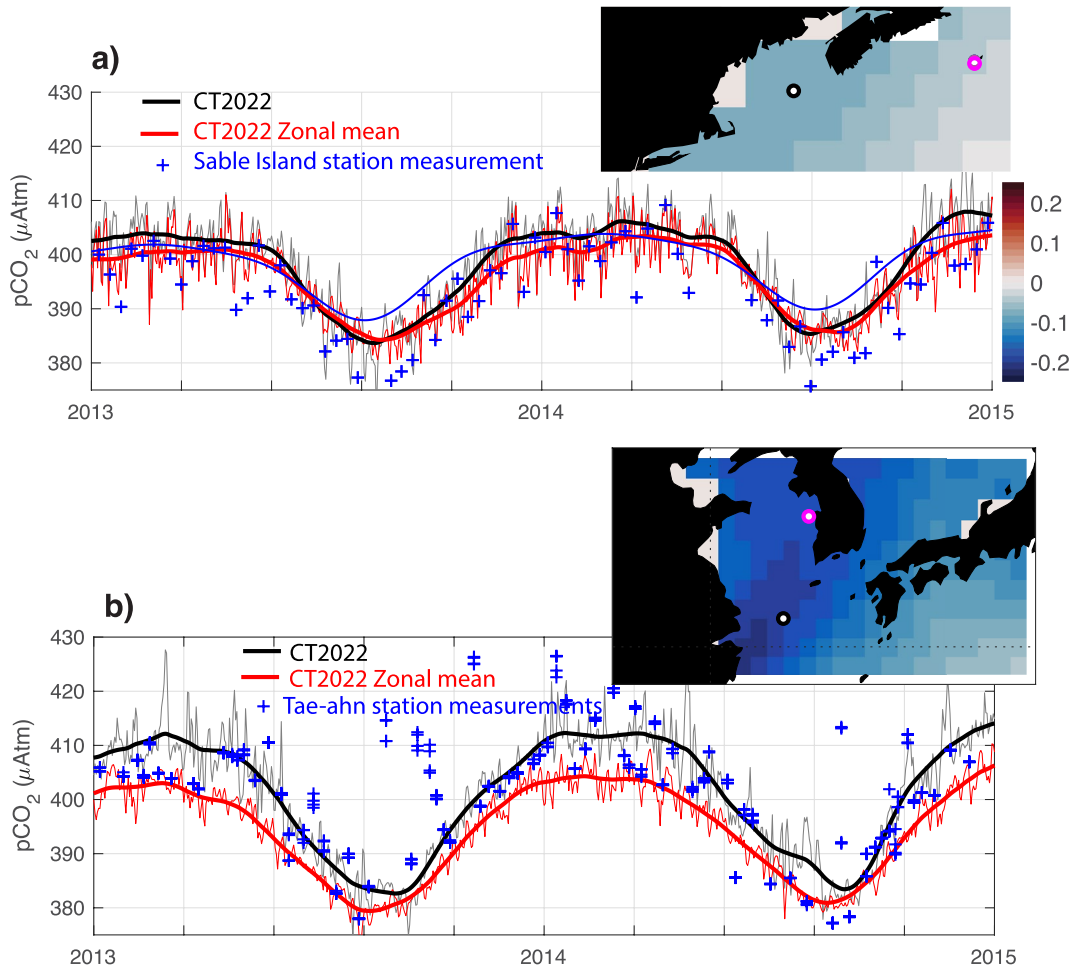

Figure 4. Example time series at two well-studied locations in *tailpipe* regions show that atmospheric pCO_2 from the CT2022 global product (black) is higher than its zonal mean at the same latitude (red). Also shown is pCO_2 calculated from direct measurements at nearby locations (blue crosses). (a) CT2022 pCO_2 (μatm) plotted for a Scotian Shelf location (43°N, 67.5°W), and measured at the Sable Island, Canada (43.9°N, 60.0°, blue crosses, plotted every 7 days) site and archived at the World Data Centre for Greenhouse Gases (https://gaw.kishou.go.jp/). The thin gray line is the 1-day mean CT2022 on the Scotian Shelf and the thick black is its 30-day running mean. The red is the same for the zonal mean of CT2022 at 43°N. The thin blue line is the empirical fit to the station data derived by Rutherford and Fennel (2022). (b) CT2022 data plotted for the East China Sea (35°N, 124.5°E, black), its zonal mean at 35°N (red) and the Tae-ahn Peninsula, South Korea and archived at the NOAA ESRL Global Monitoring Laboratory. Insets show the two study locations, including the location where the CT2022 time series is taken as a black circle and the nearby discrete measurement location as a magenta circle. Background colors in the insets are the difference between *full flux and flux with* $\chi CO_2^{\chi M\_atm}$ in 2014 (mol m^{-2} yr^{-1} colorbar applies to both insets).

over the full 19-year record are shown in Figure 3c; they all amount to greater than 10% of the daily value in the *tailpipe region*, with the locations closest to the coastline exceeding 30% during at least one day.

Overall, Figure 3 signals that process studies in regions directly adjacent to the Northern Hemisphere continents require particular care in choosing χCO_2^{atm} for the calculation of fluxes. Non-*tailpipe* regions, including west of Northern Europe, can also see large errors on a daily time frame (Figure 3c). Thus, relying on a zonal mean χCO_2^{atm} can lead to very large short-term errors and substantial underestimates for the annual uptake. Figure 4 shows two salient examples: on the Scotian Shelf east of Canada and in the East China Sea.

Rutherford and Fennel (2022) calculated air-sea fluxes over the Scotian Shelf. If they had used zonal mean χCO_2^{atm}, the regional ocean uptake would have been underestimated by 4.9% for the year 2014 (Table 2), with stronger underestimated uptake in winter. Instead, they derived atmospheric pCO_2 from the nearest existing flux station: Sable Island. A continuous approximation of the discrete Sable Island data (blue crosses, Figure 4a) was

made by fitting a seasonal cycle and linear trend to the data (thin blue curve, Figure 4a). Somewhat serendipitously, the fitted blue curve was a good approximation of the CT2022 product in 2014, because it overestimated almost all discrete flask measurement. While this approach worked well in the example year, it exemplifies the potential pitfalls of noisy and discontinuous discrete data. An inverse solution dynamically constrained and informed from all the full network of observations, like those provided by NOAA's CarbonTracker provides a promising alternative.

The flux bias that would arise from using a zonal mean atmospheric product to calculate fluxes in the East China Sea is more severe: over 17% for 2014 (Table 2). In a study of carbon fluxes in the East China Sea, Liu et al. (2022) used the discrete measurements from the nearby Tae-ahn Peninsula of South Korea (Figure 4b), which is well within the North Pacific *tailpipe region*. This choice likely minimizes bias, although the discrete measurement data is extremely noisy (Figure 4b) and the method to create a continuous time series from these discrete samples was not explained. Again, an inverse model that provides a dynamically-consistent estimate of atmospheric χCO_2 and resolves relevant gradients and temporal fluctuations is an appealing alternative to a statistical estimate from a nearby observation station.

4. Conclusions

The choice of a highly simplified zonal mean atmospheric CO_2 product, as is typical for oceanographic studies (e.g., Fay et al., 2021), embeds a bias toward underestimation of the air-to-sea transfer of CO_2 directly downwind of the industrialized continents (Figure 3). While the errors effectively cancel at basin to global scales, they cannot be ignored over *tailpipe regions* downwind of the highly industrialized North American and Asian continents (Table 2). Our effort to quantify these biases can complement work aimed at more effective monitoring of coastal ocean pCO_2 and riverine carbon fluxes.

Observations downwind of land routinely record extreme high atmospheric CO_2 anomalies (Northcott et al., 2019), as exemplified by the event recorded by three Saildrone vehicles about 30 km offshore of Rhode Island (Figure 2) and apparent in direct measurements on the Korean Peninsula (Figure 4). These *tailpipe regions* represent millions of square kilometers of ocean surface where annual ocean carbon uptake is underestimated by over 6% when a zonal mean atmospheric χCO_2 is used to calculate the flux. The bias is largest closer to land and can be as high as 30% of the flux estimate for a single day (Figure 2), highlighting the need to use an appropriate atmospheric product for local process studies or atmospheric χCO_2 whenever it is measured along with surface ocean values. Many process studies make use of the nearest location where discrete atmospheric χCO_2 is measured (e.g., Andersson et al., 2013; Liu et al., 2022; Rutherford & Fennel, 2022). This approach may improve the flux estimates relative to the use of a zonal mean, depending on the proximity to a measurement location. Yet, these discrete measurements are often collected just once or twice a month, are noisy, and may not be representative of the study location due to the presence of large gradients in atmospheric properties (Figure 4). Therefore, local process studies should either directly measure χCO_2 or consider using a product that is dynamically constrained and accounts for the vast network of direct measurements.

Conflict of Interest

The authors declare no conflicts of interest relevant to this study.

Data Availability Statement

CarbonTracker products are publicly available at: https://gml.noaa.gov/ccgg/carbontracker/. Atmospheric data from the Tae-Han observatory are archived at the NOAA ESRL Global Monitoring Laboratory (https://gml.noaa.gov/dv/data/index.php?site=TAP). Atmospheric data collected at the Sable Island observatory are archived at the World Data Centre for Greenhouse Gases (https://gaw.kishou.go.jp/search/file/0020-4019-1001-01-01-9999). Users wishing to access this data will need to register for a free login in order to gain access. Code to analyze these public data sources and make the figures in this manuscript, along with the Saildrone data used to create Figure 2, can be found at https://github.com/jpalter/Tailpipe-Manuscript/. Matlab Version R2022b was used to run these codes.

Acknowledgments
Funding for this work and LM's fellowship was provided by NSF Award #2148276 and Google.org Impact Challenge on Climate in partnership with Saildrone.com. SN gratefully acknowledges support from a URI Dean's Fellowship. The authors thank David Munroe and Andy Jacobson for helpful communications during the writing process. CarbonTracker CT2022 results provided by NOAA GML, Boulder, Colorado, USA from the website at http://carbontracker.noaa.gov.

References

Andersson, A. J., Krug, L. A., Bates, N. R., & Doney, S. C. (2013). Sea-air CO_2 flux in the North Atlantic subtropical gyre: Role and influence of sub-tropical mode water formation. *Deep Sea Research Part II: Topical Studies in Oceanography*, *91*, 57–70. https://doi.org/10.1016/J.DSR2.2013.02.022

Deike, L., & Melville, W. K. (2018). Gas transfer by breaking waves. *Geophysical Research Letters*, *45*(19), 10482–10492. https://doi.org/10.1029/2018GL078758

Fay, A. R., Gregor, L., Landschützer, P., McKinley, G. A., Gruber, N., Gehlen, M., et al. (2021). SeaFlux: Harmonization of air–sea CO_2 fluxes from surface pCO_2 data products using a standardized approach. *Earth System Science Data*, *13*(10), 4693–4710. https://doi.org/10.5194/essd-13-4693-2021

Friedlingstein, P., Jones, M. W., O'Sullivan, M., Andrew, R. M., Bakker, D. C. E., Hauck, J., et al. (2022). Global carbon budget 2021. *Earth System Science Data*, *14*(4), 1917–2005. https://doi.org/10.5194/essd-14-1917-2022

Ho, D. T., Law, C. S., Smith, M. J., Schlosser, P., Harvey, M., & Hill, P. (2006). Measurements of air-sea gas exchange at high wind speeds in the Southern Ocean: Implications for global parameterizations. *Geophysical Research Letters*, *33*(16), L16611. https://doi.org/10.1029/2006GL026817

Ho, D. T., Wanninkhof, R., Schlosser, P., Ullman, D. S., Hebert, D., & Sullivan, K. F. (2011). Toward a universal relationship between wind speed and gas exchange: Gas transfer velocities measured with $^3He/SF_6$ during the Southern Ocean Gas Exchange Experiment. *Journal of Geophysical Research*, *116*, C00F04. https://doi.org/10.1029/2010JC006854

Jacobson, A. R., Schuldt, K. N., Tans, P., Andrews, A., Miller, J. B., Oda, T., et al. (2023). *CarbonTracker CT2022*. NOAA Global Monitoring Laboratory. https://doi.org/10.25925/Z1GJ-3254

Jersild, A., Landschützer, P., Gruber, N., & Bakker, D. C. E. (2023). An observation-based global monthly gridded sea surface pCO_2 and air-sea CO_2 flux product from 1982 onward and its monthly climatology (NCEI Accession 0160558). Version 7.7 [Dataset]. *NOAA National Centers for Environmental Information*. https://doi.org/10.7289/v5z899n6

Landschützer, P., Gruber, N., & Bakker, D. C. E. (2016). Decadal variations and trends of the global ocean carbon sink. *Global Biogeochemical Cycles*, *30*(10), 1396–1417. https://doi.org/10.1002/2015gb005359

Landschützer, P., Gruber, N., Bakker, D. C. E., Schuster, U., Nakaoka, S., Payne, M. R., et al. (2013). A neural network-based estimate of the seasonal to inter-annual variability of the Atlantic Ocean carbon sink. *Biogeosciences*, *10*(11), 7793–7815. https://doi.org/10.5194/bg-10-7793-2013

Landschützer, P., Laruelle, G. G., Roobaert, A., & Regnier, P. (2020). A uniform pCO_2 climatology combining open and coastal oceans. *Earth System Science Data*, *12*(4), 2537–2553. https://doi.org/10.5194/essd-12-2537-2020

Liu, J., Bellerby, R. G. J., Li, X., & Yang, A. (2022). Seasonal variability of the carbonate system and air–sea CO_2 flux in the outer Changjiang Estuary, East China Sea. *Frontiers in Marine Science*, *8*, 765564. https://doi.org/10.3389/fmars.2021.765564

Nickford, S., Palter, J. B., Donohue, K., Fassbender, A. J., Gray, A. R., Long, J., et al. (2022). Autonomous wintertime observations of air-sea exchange in the Gulf Stream reveal a perfect storm for ocean CO_2 uptake. *Geophysical Research Letters*, *49*(5), e2021GL096805. https://doi.org/10.1029/2021GL096805

Northcott, D., Sevadjian, J., Sancho-Gallegos, D. A., Wahl, C., Friederich, J., & Chavez, F. P. (2019). Impacts of urban carbon dioxide emissions on sea-air flux and ocean acidification in nearshore waters. *PLoS One*, *14*(3), e0214403. https://doi.org/10.1371/journal.pone.0214403

Peters, W., Jacobson, A. R., Sweeney, C., Andrews, A. E., Conway, T. J., Masarie, K., et al. (2007). An atmospheric perspective on North American carbon dioxide exchange: CarbonTracker. *Proceedings of the National Academy of Sciences*, *104*(48), 18925–18930. https://doi.org/10.1073/pnas.0708986104

Rutherford, K., & Fennel, K. (2022). Elucidating coastal ocean carbon transport processes: A novel approach applied to the northwest North Atlantic Shelf. *Geophysical Research Letters*, *49*(6), e2021GL097614. https://doi.org/10.1029/2021GL097614

Sabine, C., Sutton, A., McCabe, K., Lawrence-Slavas, N., Alin, S., Feely, R., et al. (2020). Evaluation of a new carbon dioxide system for autonomous surface vehicles. *Journal of Atmospheric and Oceanic Technology*, *37*(8), 1305–1317. https://doi.org/10.1175/JTECH-D-20-0010.1

Sabine, C. L., Feely, R. A., Gruber, N., Key, R. M., Lee, K., Bullister, J. L., et al. (2004). The oceanic sink for anthropogenic CO_2. *Science*, *305*(5682), 367–371. https://doi.org/10.1126/science.1097403

Sutton, A. J., Williams, N. L., & Tilbrook, B. (2021). Constraining Southern Ocean CO_2 flux uncertainty using uncrewed surface vehicle observations. *Geophysical Research Letters*, *48*(3), e2020GL091748. https://doi.org/10.1029/2020GL091748

Wanninkhof, R. (2014). Relationship between wind speed and gas exchange over the ocean revisited. *Limnology and Oceanography: Methods*, *12*(6), 351–362. https://doi.org/10.4319/lom.2014.12.351

Wanninkhof, R., Pickers, P. A., Omar, A. M., Sutton, A., Murata, A., Olsen, A., et al. (2019). A surface ocean CO_2 reference network, SOCONET and associated marine boundary layer CO_2 measurements. *Frontiers in Marine Science*, *6*, 400. https://doi.org/10.3389/fmars.2019.00400

Yamamoto, A., & Palter, J. B. (2016). The absence of an Atlantic imprint on the multidecadal variability of wintertime European temperature. *Nature Communications*, *7*(1), 10930. https://doi.org/10.1038/ncomms10930